Vibrational properties of ferroelectric β-vinylidene fluoride polymers and oligomers

Serge M. Nakhmanson
Materials Science Division, Argonne National Laboratory, Argonne, Illinois 60439, USA

R. Korlacki, J. Travis Johnston, and Stephen Ducharme*
Department of Physics and Astronomy and the Nebraska Center for Materials and Nanoscience, University of Nebraska–Lincoln, Lincoln, Nebraska 68588-0111, USA

Zhongxin Ge and James M. Takacs
Department of Chemistry and the Nebraska Center for Materials and Nanoscience, University of Nebraska–Lincoln, Lincoln, Nebraska 68588-0113, USA

(Received 23 December 2009; revised manuscript received 27 February 2010; published 27 May 2010)

We utilize a plane-wave density-functional theory approach to investigate the vibrational properties of the all-*trans* ferroelectric phase of poly(vinylidene fluoride) (β-PVDF) showing that its stable state corresponds to the *Ama*2 structure with ordered dihedral tilting of the VDF monomers along the polymer chains. We then combine our theoretical analysis with IR spectroscopy to examine vibrations in oligomer crystals that are structurally related to the β-PVDF phase. We demonstrate that these materials—which can be grown in a highly crystalline form—exhibit IR activity similar to that of β-PVDF, making them an attractive choice for the studies of electroactive phenomena and phase transitions in polymer ferroelectrics.

DOI: 10.1103/PhysRevB.81.174120 PACS number(s): 61.41.+e, 36.20.Ng, 77.80.−e, 77.84.Jd

I. INTRODUCTION

The best-known ferroelectric polymer, polyvinylidene fluoride (PVDF),[1,2] is widely used in applications ranging from loudspeakers to ultrasound transducers, owing to its large piezoelectric response combined with low cost, ease of processing, and chemical inertness.[3] PVDF stands out among the small number of known ferroelectric polymers mainly due to the compactness and mechanical simplicity of the alkanelike linear molecular structure, which affords both good crystallinity[4] and facile dipole rotation.[5] The ferroelectric or β phase of PVDF consists of a quasihexagonal close-packed crystalline arrangement of polymer chains having an all-*trans* conformation with all the -CF_2-CH_2- molecular units aligned along a single polar axis [see Fig. 1(a)].[6–8] Conceptually, β-PVDF can be regarded as an elementary model for polymer ferroelectricity that lends itself well to studies with predictive computational methods, such as density-functional theory (DFT), and can be used as a basis for detailed understanding of more complicated compounds. However, experimentally grown PVDF samples usually require extensive postprocessing to become ferroelectric and even at this stage they remain far from being perfectly ordered.[4] The nature of the high-temperature phase transition of β-PVDF into a nonpolar state is also unclear as the polar structure melts before reaching it. This complication can be avoided by copolymerizing vinylidene fluoride with other molecules, e.g., with trifluoroethylene,[9,10] which decreases the ferroelectric-to-paraelectric (F-P) transition temperature and it has been shown that the high-temperature nonpolar phase in such systems consists of a disordered alternating *trans-gauche* conformation.[7,11]

The recent demonstration of ferroelectricity in VDF oligomer crystals[12,13] (OVDF) is a significant development that could further our insight into the nature of polymer ferroelectricity. The oligomers consist of linear VDF chains with lengths ranging from a few to a few dozen VDF molecules and terminated by various other molecular units at the ends. They appear to be functionally equivalent to PVDF but are easier to process with a variety of fabrication techniques. They also crystallize well by evaporation,[14] with the degree of crystallinity at least comparable to those of PVDF-copolymer structures.[13] There is hope that well-ordered oligomer samples will exhibit clear F-P transitions, thus providing valuable information about the nature of the high-temperature nonpolar phase for this class of polymeric materials.

Although there has been much progress in understanding the phenomenology of PVDF and its copolymers,[15–17] compared to the body of work devoted to similar studies of ferroelectric complex oxides,[18] relatively little is known about the mechanisms responsible for polymer ferroelectricity at the microscopic level. Models based on mean-field theory have been useful in describing the physical properties[19,20] but yield little insight into the role of molecular interactions in stabilizing the ferroelectric state. Empirical molecular-dynamics models,[21–25] on the other hand, lack the detailed quantum-mechanical rigor and predictive power of first-principles-based methods, which have achieved spectacular success in explaining the microscopic underpinnings of ferroelectricity in complex-oxide materials.[18] Therefore, a more comprehensive approach to the atomistic-level studies of structural, polar (polarization and piezoelectricity), and dynamical (dielectric constants and phase transitions) properties of ferroelectric polymers would incorporate the usage of first-principles-based techniques and, in certain cases, heavily borrow from the methodological developments introduced for the simulations of complex oxides. Recent examples of such a hybrid approach to investigations of the ferroelectric-polymer systems include predictive evaluation of the properties of PVDF,[26,27] VDF copolymers,[28] and

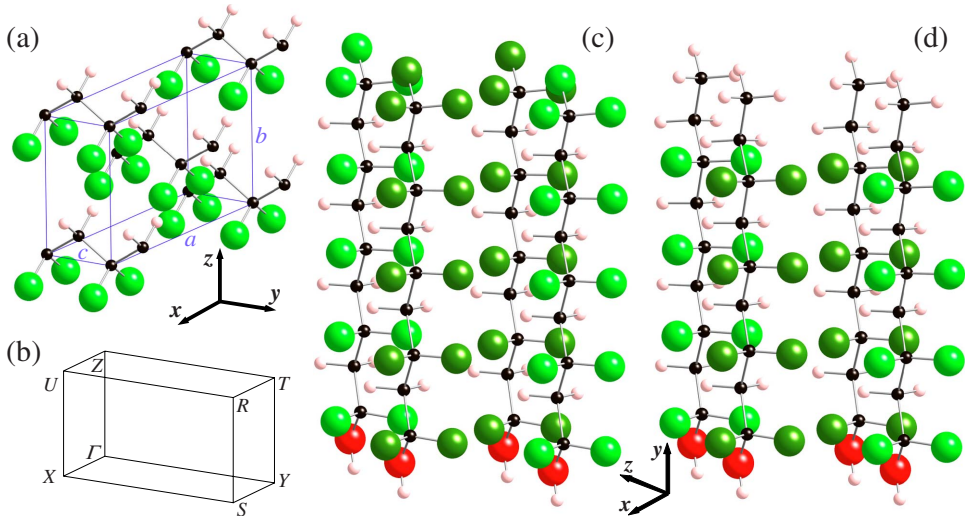

FIG. 1. (Color online) (a) The structure of the orthorhombic *Pmm*2 β-PVDF cell with two VDF monomers. Extra monomers are shown to illustrate how the all-*trans* polymer chains are formed by applying the PBC along the *y* direction. (b) The sketch of a positive octant of the *Pmm*2 BZ referred to the same coordinate axes as in (a). [(c) and (d)] The $n=4$ oligomer systems with the OH- bottom and CF_3- and CH_3- top anchoring units. H and C atoms are represented by small white and black spheres, respectively. F atoms are represented by large spheres of two different shades to better distinguish individual oligomer chains.

PVDF analogs,[27,29] as well as the computation of their vibrational spectra.[30–32]

In this paper, using DFT techniques, we evaluate the stability of the highly symmetric *Amm*2 ferroelectric β-PVDF phase. We find that its dynamically stable configuration includes a slight distortion away from this symmetry in a form of an ordered dihedral-tilt angle staggering along the polymer backbone. This distortion provides a microscopic-level underpinning for the stiffening phase transition that was experimentally observed in PVDF at 160 K by inelastic neutron scattering.[33] Then, by doing simulations for periodic molecular chain arrangements as well as for individual chains, we investigate the vibrational properties of several VDF oligomer structures, demonstrating that they behave similarly to the β-PVDF.

The rest of the paper is organized as follows. In Sec. II we thoroughly flesh out the motivations for vibrational studies of VDF polymers and oligomers, and complement them with the description of the technical details of our computational approach. In Sec. III we discuss the results of our simulations of vibrations in the ferroelectric β-PVDF and VDF-oligomer crystals, and individual VDF-oligomer chains. We conclude in Sec. IV, presenting a brief summary of the results of our studies.

II. MOTIVATIONS AND METHODOLOGY

Lattice instabilities in ferroelectric materials are intimately linked to their structural and electroactive properties.[34] The important consequences of their influence on the material's behavior and physical characteristics have been exhaustively studied for most prototypical perovskite-oxide ferroelectrics,[35–38] shedding light onto the microscopic origins of their F-P phase transitions. It is, however, unknown if the lattice-instability analysis could be applied to the high-temperature nonpolar phase of PVDF, as it is unclear exactly which structural model—out of all the possible nonpolar arrangements of various conformations of the VDF polymer chains (that could also be statically and/or dynamically disordered)—should be utilized as its starting point. More importantly, the whole view of such a phase transition as freezing in of a soft vibrational mode may not be applicable. It is, nevertheless, tempting to apply that powerful technique to this polymer system, and in what follows we use it to evaluate the stability of the highly symmetric, or the so-called "planar-zigzag," *Amm*2 ferroelectric phase of PVDF. This approach allows one to unequivocally determine the local minimum-energy configuration for polar PVDF, at least on the level of standard DFT-based techniques available in most modern computational packages. (Until now, either accepting or rejecting the simple argument of Hasegawa *et al.*,[39] various authors use either the planar zigzag[27,28,30,31,40] or the so-called "alternately deflected"[41] configurations as their structural models for ferroelectric β-PVDF.[42]) Furthermore, we can then compare the vibrations obtained for such perfectly ordered models of β-PVDF with the results of both theoretical and experimental investigations of the OVDF systems and establish whether the dynamical properties of the former and the latter have any resemblance.

The details of our computational approach are the following. A conventional orthorhombic unit cell, characterized by lattice constants *a*, *b*, and *c* [see Fig. 1(a)], was used to compute phonon bands in the planar-zigzag β-PVDF structure. The cell contains two six-atom VDF monomers that are "polymerized" into infinite chains by applying periodic boundary conditions (PBCs) along the *y* axis, which we choose as the polymer-backbone direction. The *z* axis is set as the principal direction of the VDF-monomer dipole moments. Depending on whether or not we consider the two chains to be connected by a $(\frac{1}{2}a, \frac{1}{2}b)$ translation in the *xz*

plane, the structure's symmetry could be regarded as either *Amm*2 or *Pmm*2. Unit cells for oligomer systems are constructed in the similar fashion and with the same convention for choosing z and y axes. The cells are orthorhombic in shape (deviations from the orthorhombic symmetry[43] are not considered in this investigation) and contain two finite oligomer chains, each consisting of n VDF monomers connected with top and bottom anchoring units. With PBC applied along the y axis, i.e., in the oligomer-chain backbone direction, layered oligomer crystals are formed by stacking individual quasi-two-dimensional oligomer slabs, like the ones shown in Figs. 1(b) and 1(c), on top of each other.

We have used a DFT-based plane-wave method QUANTUM ESPRESSO (QE) (Ref. 44) and Vanderbilt ultrasoft pseudopotentials[45] for the relaxation of ionic positions and stress-tensor components $\sigma_{\alpha\beta}$ (with the orthorhombic symmetry enforced) of the simulation cells. The phonon frequencies were computed with the help of a density-functional perturbation-theory approach.[46] The exchange-correlation interaction was described by the generalized gradient approximation functional of Perdew, Burke, and Ernzerhof (PBE).[47] The electronic wave function and density plane-wave cutoffs were 30 Ry and 300 Ry, respectively. The systems were considered to be at equilibrium when the forces on the ions were less than 0.4×10^{-3} Ry/bohr ($\sim$0.01 eV/Å) and the $\sigma_{\alpha\alpha}$ components of the stress tensor were smaller than 0.5 kbar. For the 12-atom β-PVDF cell, $2\times8\times4$ and $4\times8\times6$ Monkhorst-Pack (MP) meshes[48] were used for the Brillouin zone (BZ) integrations and for phonon-band calculations, respectively [see Fig. 1(b) for a sketch of a positive octant of the *Pmm*2 BZ]. For β-PVDF cells doubled along the y direction, we used $2\times4\times4$ and $2\times2\times2$ MP meshes, i.e., phonons were computed only at Γ and the BZ-boundary points. Finally, for the oligomer systems, a $2\times1\times4$ MP mesh was employed for the BZ integrations and phonons were evaluated only at Γ point.

Computed phonon spectra for oligomer crystals were complemented by similar calculations for individual VDF-oligomer molecules *in vacuo* performed using DFT, as implemented in a quantum chemistry code PQS.[49] The same PBE (Ref. 47) density functional was employed to account for exchange and correlation interactions and the split-valence set 6-31++G(d,p) (Ref. 50) was used as a basis set for the wave-function decomposition.[51,52] The accuracy of integration in the self-consistent field (SCF) procedure was kept at 10^{-8} and 10^{-12} for preliminary and final iterations, respectively. The SCF convergence threshold was 10^{-6} for the maximum Brillouin matrix element at convergence. The convergence criteria for the geometry optimization were as follows: maximum allowed gradient component $<$0.0003 a.u. and energy change from previous cycle $<10^{-6}$ hartree. No particular symmetry was enforced during the optimization, as doing so for an isolated molecule results in an unstable structure with numerous imaginary modes. However, when no symmetry constraints are imposed, in the absence of the stabilizing crystal field the repulsive interactions among the negatively charged fluorine atoms lead to an artificial deformation of the molecule's geometry. Depending on the size and shape of the basis functions used, the molecules may become bent (see, e.g., Ref. 53) or twisted (this investigation using a basis set with diffuse functions).

TABLE I. Comparison between the experimental and theoretical lattice constants (in angstrom) for the orthorhombic β-PVDF unit cell.

	Expt.[a]	Calc.
a	8.58	8.55
b	4.91	4.83
c	2.56	2.58

[a]Reference 11.

Unlike in the situation with most "hard" materials, vibrational frequencies obtained for organic systems using various computational techniques, including DFT, systematically deviate from the experimental data by a few percent.[54–56] This happens primarily due to the neglect of anharmonicity effects and is most noticeable at higher frequencies, especially if the atoms involved in the corresponding vibrations are light. Additional sources of errors can also be ascribed to approximations in the treatment of electronic exchange and correlation effects, and the quality of the employed basis sets and pseudopotentials. The frequency drifts are strongly dependent on a particular computational method used and could be corrected by a direct rescaling by an empirical factor.[54–58] In this investigation, we have rescaled the "raw" frequencies from the periodic calculations with QE by applying two scaling factors: 1.0427 in the low-frequency region under 2000 cm^{-1} and 0.9879 for the high-frequency stretching vibrations involving heavy atoms and hydrogen around 3000 cm^{-1} (these modes are usually strongly anharmonic and it is beneficial to treat them separately, see Ref. 57). These scaling factors were optimized for the OVDF systems to minimize the deviations between the calculated and experimental frequencies of the major IR active vibrational modes (listed in Table II). We then used the same scaling factors to refine the computed frequencies for the PVDF and the isolated-chain OVDF systems.

Finally, in order to simulate the oligomer IR spectra for the crystalline and isolated-chain systems and to compare them with the experimental results, we have broadened the computed frequencies by overlapping them with Gaussian peaks that were 10 cm^{-1} wide. In a few cases modes with similar IR intensities were located very close to each other and thus not distinguishable in such broadened spectra. We treated such bands as one, i.e., listed only the averaged central frequency of the broadened peak in Table II, which makes the comparison with experiments more straightforward. We also included all the significant components of such bands in the potential-energy distribution (PED) analysis using their computed intensities as relative weights.

III. RESULTS AND DISCUSSION

A. Vibrations in β-PVDF polymer crystal

In this section we present the results of our calculations of the structural and vibrational properties of the β-PVDF polymer crystal. The equilibrium lattice constants for the relaxed

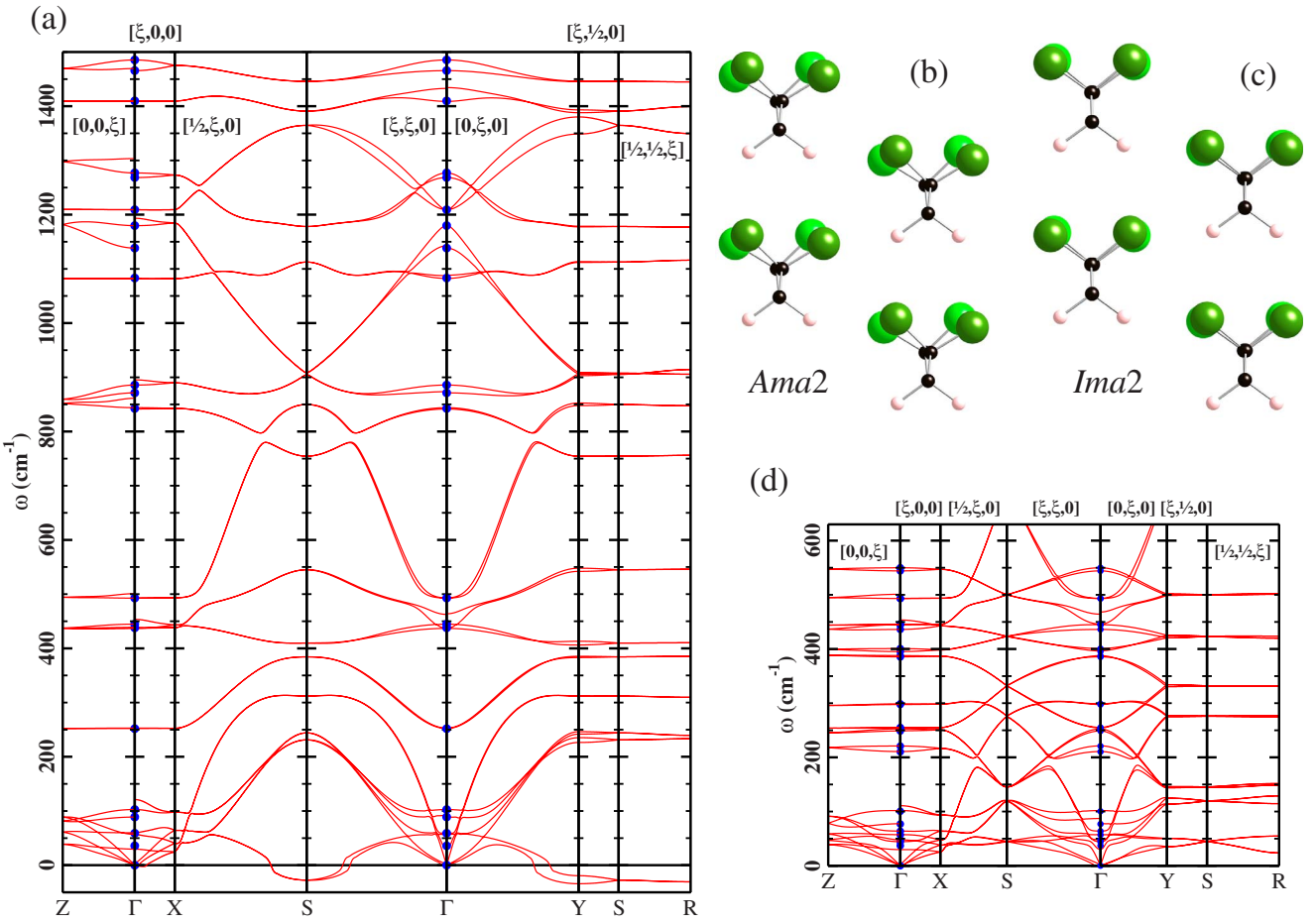

FIG. 2. (Color online) (a) Dispersion of the phonon bands in the 12-atom orthorhombic β-PVDF unit cell along the symmetric directions in the *Pmm*2 BZ, outlined in Fig. 1(b). High-frequency bands in the vicinity of 3000 cm^{-1} are not shown. [(b) and (c)] Sketches of the VDF monomer tilting patterns produced by freezing-in of the (b) Y_1 and (c) Y_2 structural instabilities, viewed along the backbone (y) direction. Color conventions are the same as for Fig. 1. (d) Dispersion of the phonon bands for the relaxed cell-doubled *Ama*2 β-PVDF crystal with the frozen-in Y_1 structural instability. Only the low-frequency bands are shown. In the panels (a) and (d), dots placed along the frequency axis at Γ point indicate phonon frequencies computed with vanishing LO-TO splitting. All the phonon frequencies shown here were rescaled with an empirical factor. See text for more details.

orthorhombic *Amm*2 β-PVDF structure, shown in Fig. 1(a), are listed in Table I and exhibit good agreement with experimental results. In Fig. 2(a) we show the phonon-dispersion curves computed for this system along a number of high-symmetry directions in its *Pmm*2 BZ, as outlined in Fig. 1(b).[62] The unstable modes have imaginary frequencies and their dispersion is shown below the zero-frequency line. Our calculations indicate that, although the planar-zigzag system is stable at Γ point, it has multiple structural instabilities confined to quasi-one-dimensional regions of reciprocal space spanning along, e.g., the *Y*-*S* and *S*-*R* BZ edges: a strikingly similar trend to the one observed in the lattice dynamics of the high-temperature (cubic) phases for a number of generic perovskite-oxide materials.[36,37] Specifically, at *Y* point, the system has two unstable modes at $34i$ and $19i$ cm^{-1} (called in what follows Y_1 and Y_2), both having B_1 symmetry. The schematic views of the phonon eigenvectors, or atomic-displacement motifs, corresponding to these instabilities are shown in panels (b) and (c) of Fig. 2 for Y_1 and Y_2, respectively. In both cases, the freezing-in of the particular structural instability corresponds to dihedral tilting of the VDF monomers along the polymer chains. For the Y_1 distortion these tilts are the same for both polymer chains in the unit cell, resulting in the alternately deflected structure with the *Ama*2 symmetry. For the Y_2 distortion the tilts of the monomers belonging to one of the chains are mirror images of the ones belonging to the other chain, which results in a structure possessing an *Ima*2 symmetry. The freezing-in of either of the *Y*-point distortions leads to doubling of the original 12-atom cell along the y axis and folding of the *Y*-*S*-*R*-*T* boundary region of its *Pmm*2 BZ back into the Γ-*X*-*U*-*Z* region. We have checked the stability of both cell-doubled structures, produced by first freezing-in the appropriate Y_i instability with a small amplitude and then relaxing the distorted system to small ionic forces and stresses. In both cases, the relaxation produced only negligible changes in the lattice constants. In Fig. 2(d) we present the phonon-dispersion curves computed for the alternately deflected *Ama*2 structure with the frozen-in Y_1 instability, traced along the same directions in the *Pmm*2 BZ as for the original highly symmetric phase. Our analysis indicates that this structure is stable everywhere across the BZ and, conse-

TABLE II. Major IR-active vibrational modes computed for the β-PVDF crystal and OVDF $n=6$ crystal, and isolated chain with OH-bottom and CF_3- top terminating units. Experimental OVDF data are for the $n=6$ crystal terminated with CF_3- and iodine. All frequencies ω are given in cm^{-1}. Mode assignments are based on the PED analysis. They do not sum up to 100% because only significant contributions (exceeding 5%) are listed. Key: ν—stretching (s—symmetric, a–antisymmetric), δ—bending, w—wagging, r—rocking, σ—scissoring, t—twisting, and τ—torsion. The sign + or − denotes the phase relation among the symmetry coordinates (as in Ref. 59).

PVDF								OVDF ($n=6$)				
Expt. Ref. 59	Force-field analysis Ref. 59			DFT calculation				DFT calculation				Expt.
				QE, *Amm*2		QE, *Ama*2		QE, crystal		PQS, chain		
ω	ω	Irrep.	Assignment	ω	Irrep.	ω	Irrep.	ω	Assignment	ω	Assignment	ω
70[a]	77[a]	B_2[a]	Librational lattice mode[a]	89	B_1	77	B_1	91	Librational lattice mode	-	-	-
260	265	A_2	$t(CF_2)(100)$	-	-	-	-	242	$t(CF_2)(72)+\tau(CCCF)(12)+r(CH_2)(6)$	-	-	-
442	444	B_2	$r(CF_2)(70)+r(CH_2)(24)$	438	B_2	-	-	447	$\nu_a(CF_2)(47)+r(CF_2)(49)$	412	$\nu_a(CF_2)(38)+r(CF_2)(27)+\nu_a(CC)(26)$	-
468	471	B_1	$w(CF_2)(90)$	445	B_1	445	B_1+B_2	469	$\nu_a(CC)(66)+w(CF_2)(16)+\sigma(CF_2)(7)$	492	$\nu_a(CC)(40)+\nu(CF_2)(23)+\sigma(CF_2)(21)+w(CF_2)(7)$	466[b]
508	513	A_1	$\delta(CF_2)(98)$	493	A_1	493	A_1	490	$\nu_s(CF_2)(34)+\nu(CC)(18)+\sigma(CF_2)(29)+\delta(CCC)(5)$	507	$\nu_s(CF_2)(30)+\nu(CC)(25)+\sigma(CF_2)(17)+w(CF_2)(10)$	507
840	844	A_1	$\nu_s(CF_2)(59)+\nu(CC)(17)$	842	A_1	842	A_1	838	$\nu_s(CF_2)(80)+\nu_s(CC)(13)$	854	$\nu_s(CF_2)(79)+\nu_s(CC)(16)$	838
880	883	B_2	$r(CH_2)(62)-\nu_a(CF_2)(18)-r(CF_2)(19)$	871	B_1	870	B_1	866	$\nu_a(CF_2)(91)$	894	$\nu_a(CF_2)(88)+r(CF_2)(6)$	879
1071	1074	B_1	$\nu_a(CC)(53)+w(CH_2)(25)-w(CF_2)(22)$	1083	B_2	1088	B_2	1063	$\nu_s(CF_2)(52)+\nu_a(CC)(46)$	1075	$\nu_a(CC)(59)+\nu_s(CF_2)(37)$	1077
1177	1177	B_2	$\nu_a(CF_2)(71)-r(CF_2)(18)$	1138	B_1	1139	B_1	1143	$\nu_a(CF_2)(92)$	1214	$\nu_a(CF_2)(89)+\nu_a(CC)(7)$	1162
1273	1283	A_1	$\nu_s(CF_2)(40)-\nu_s(CC)(22)+\delta(CCC)(26)$	1269	A_1	1270	A_1	1270	$\nu_s(CF_2)(60)+\nu_s(CC)(31)$	1288	$\nu_s(CF_2)(75)+\nu_s(CC)(17)$	1273
1398	1408	B_1	$w(CH_2)(58)-\nu_a(CC)(34)$	1410	B_2	1414	B_2	1425	$\nu_a(CC)(84)$	1414	$\nu_a(CC)(85)$	1402
1428	1434	A_1	$\delta(CH_2)(81)$	1466	A_1	1467	A_1	1469	$\nu(CO)(39)+\nu(CC)(25)+\sigma(CH_2)(17)+\nu_s(CF_2)(10)$	1454	$\nu(CO)(44)+\nu(CC)(37)+\nu_s(CF_2)(11)$	1431
2980	2975	A_1	$\nu_s(CH_2)(99)$	2971	A_1	2971	A_1	2973	$\nu_s(CH_2)(99)$	2976	$\nu_s(CH_2)(99)$	2979
3022	3024	B_2	$\nu_a(CH_2)(99)$	3025	B_1	3024	B_1	3021	$\nu_a(CH_2)(99)$	3028	$\nu_a(CH_2)(99)$	3015

[a]From Ref. 60.
[b]From Ref. 61.

quently, is the low-temperature minimum-energy configuration for the β-PVDF polymer crystal. A similar check performed for the frozen-in-Y_2 *Ima*2 structure (results not shown) reveals that it remains unstable and thus cannot be the minimum-energy state for β-PVDF.

The computed IR mode frequencies for the *Amm*2 and *Ama*2 β-PVDF structures are given in the left part of Table II. Previous experimental and empirical force-field modeling results of Tashiro *et al.*[59] are included for comparison. Our calculations show that the IR-active modes at frequencies above 400 cm^{-1} are insensitive to the presence of the Y_1 dihedral-angle staggering distortion and exhibit good agreement with experimental results. Taking into account the experimental evidence for the stiffening transition observed at 160 K in crystalline copolymer films of VDF (70%) and trifluoroethylene (30%),[33] we can envision the following approximate phase diagram for β-PVDF at temperatures below melting. At low T the system has the *Ama*2 symmetry with ordered dihedral tilting of VDF units along the chains, as demonstrated by the instability analysis. At elevated T a softening transition occurs, indicating that the dihedral VDF-unit tilts either disappear or disorder, and the system displays the *Amm*2 symmetry in diffraction.

Finally, we should also mention that the "softness" of the Y_1 mode (i.e., the largeness of its imaginary frequency) is relatively weak, compared to the lattice instabilities typically found in calculations for perovskite-oxide ferroelectrics.[35–38] It is quite possible that this mode's behavior will strongly depend on the details of DFT calculations, particularly on the quality of employed pseudopotentials, the type of exchange-and-correlation functional used and the accuracy of converging the stress-tensor components to low values when determining the equilibrium lattice constants.

B. Vibrations in VDF oligomers

As VDF oligomers are structurally similar to PVDF,[12,14,63] their vibrational properties would be expected to resemble those of their polymer prototype, with contributions from the anchor-unit vibrational modes becoming weaker with increasing length of the oligomer chains. Previous studies of OVDF indicate that the formation of different crystal phases, attributed to be analogous of α, β, and γ phases of PVDF, can be facilitated by altering the oligomer-chain length or termination and by adjusting the sample preparation procedures.[14,61,63–65] Here we present the results of our investigation of the vibrational properties of the all-*trans* conformation of ferroelectric OVDF, which is equivalent to the β phase of PVDF. We have considered six different OVDF crystals with the number of VDF monomers n along the chain equal to 4, 6, and 8, and we have used OH-, CF_3-, and CH_3- molecules as the bottom and two variants of top anchoring units, respectively. Analogously to the *Amm*2 planar-zigzag β-PVDF case, in all the calculations for the OVDF crystals we force the individual oligomer-chain backbones to be planar, with the backbone planes also being mirror planes. Since OVDF-crystal unit cells contain complete molecular chains, all vibrations analogous to those dispersed along the Γ-Y line in the β-PVDF case (including ones corresponding to the Y_1 and Y_2 dihedral-angle staggering modes) would be folded into Γ point of the OVDF-crystal BZ and thus accessible in our calculations.

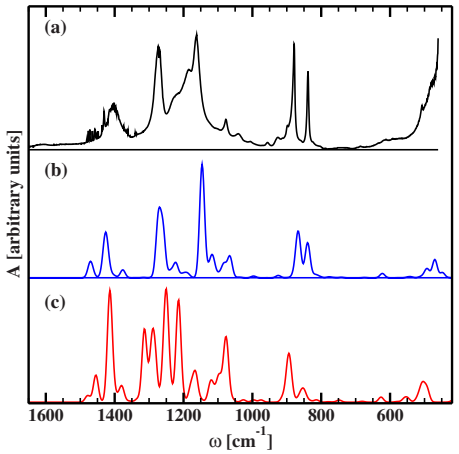

FIG. 3. (Color online) Comparison of simulated and experimental IR spectra for the $n=6$ OVDF structure, terminated with CF_3- on one end and either OH (simulated) or iodine (experimental) on the other. All spectra are normalized to the strongest peak and shifted for clarity. (a) Experimental spectrum, (b) crystal calculation with QE, and (c) isolated-chain calculation with PQS.

To make comparisons with our OVDF vibrational calculations, we acquired a reference experimental spectrum of an $n=6$ OVDF crystal with chains terminated by CF_3- and iodine. The sample has been synthesized by iodine transfer polymerization according to a procedure published elsewhere.[66–68] The sample was prepared as a capillary cell using two zinc selenide substrates and a Mylar foil 6 micrometers thick as spacers, and filled with pure oligomer by the capillary effect a few degrees above the melting point and then cooled down. The absorption spectrum was recorded at room temperature using a Thermo Nicolet 380 Fourier transform infrared spectrometer, with spectral resolution of 1 cm^{-1} and accumulation of 32 scans. The transmission characteristic of the substrates and the spectrometer optics limited the spectral window to the range above 500 cm^{-1}.

The obtained experimental and computational IR-mode data for the $n=6$ OVDF structure is summarized in the left part of Table II, with the associated IR spectra shown in Fig. 3. Computed IR properties of other OVDF structures considered in this investigation are similar to this representative system and are not shown separately. Both periodic and isolated-chain DFT calculations for CF_3-$(VDF)_6$-OH produce consistent results, with the average deviations of frequencies of major IR modes from the experimental values being 13 cm^{-1} and 14 cm^{-1}, respectively, after empirical scaling. For comparison, the classical valence force field developed in Ref. 59 produces an average frequency deviation of only 5 cm^{-1}, however, it was explicitly fitted to reproduce the experimental IR spectrum of β-PVDF that was obtained in the same project.

It is worth pointing out that, compared to the experiment, the computed oligomer-crystal IR spectrum in Fig. 3 is lacking a shoulder in the vicinity of 1200 cm^{-1}, between two

strong peaks that are well reproduced by the calculation. This shoulder is, however, filled in by a several strong features clearly present in the simulated spectrum of the isolated chain. This frequency interval is dominated by the skeletal carbon-backbone vibrations, suggesting that such modes are amplified in isolated chains and suppressed in the periodic systems. We can then conclude that the experimental sample used to obtain the IR spectrum in Fig. 3 is not completely crystalline, with disordered parts behaving more like arrangements of individual oligomer molecules.

In general, comparing the vibrational data for all of the six OVDF structures considered here with that of the β-PVDF, we observe the following trends. (i) In the frequency range above 400 cm^{-1}, the IR-active frequencies for β-PVDF and OVDF structures computed with QE are essentially the same. (ii) At lower frequencies, all the OVDF structures, as well as the β-PVDF structure, have an IR-active librational lattice mode in the 75–90 cm^{-1} frequency region, which was discussed in Ref. 60. (iii) The $n=4$ and $n=6$ OVDF structures with shorter chains exhibit no analogs of the soft $Y_{1,2}$ dihedral-angle staggering modes while the $n=8$ longer-chain ones do, indicating that there is a crossover in the OVDF equilibrium behavior from the planar-zigzaglike (oligomer-chain backbone lies in a plane that is also a mirror plane) to the alternately deflectedlike (oligomer-chain backbone is no longer planar and the mirror plane is broken) structure as the oligomer chains grow in length.

IV. CONCLUSIONS

To conclude, we have used a hybrid approach combining first-principles simulations with plane-wave DFT methods and IR spectroscopy to investigate the vibrational properties and structural stability of the ferroelectric β phase of PVDF and OVDF crystals based on this phase. For the β-PVDF we find that the dynamically stable minimum-energy state corresponds to the alternately deflected *Ama*2 structure with ordered dihedral tilts of VDF monomers along the polymer chains. All of the oligomer systems that we have considered possess essentially the same IR activity signatures as the β-PVDF at frequencies above 400 cm^{-1}, allowing us to conclude that their vibrational behavior is very similar to their polymeric prototype. At low frequencies, we observed a stability crossover from a structure with no dihedral tilts to a structure with developed dihedral tilts as the length of the oligomer chains increased from six to eight VDF units. Since the experimental samples of these simple materials can be grown with the same or even better degree of crystallinity as that of the PVDF-copolymer compounds, they could be utilized as convenient test cases for the studies of ferroelectric phenomena and ferroelectric-to-paraelectric phase transitions in polymers, as well as be integrated into a variety of flexible state-of-the-art nanoelectromechanical devices.

ACKNOWLEDGMENTS

The authors gratefully acknowledge financial support of the Department of Energy. S.M.N. was supported by the U.S. Department of Energy, Office of Science, Office of Basic Energy Sciences under Contract No. DE-AC02-06CH11357. Work at the University of Nebraska was supported by the DOE under Grant No. DE-FG02-08ER46498 and by the Nebraska Research Initiative. Part of the computations was completed using resources of the Holland Computing Center at the University of Nebraska-Lincoln.

*sducharme1@unl.edu

[1] H. Kawai, Jpn. J. Appl. Phys. **8**, 975 (1969).
[2] A. J. Lovinger, Science **220**, 1115 (1983).
[3] T. T. Wang, J. M. Herbert, and A. M. Glass, *The Applications of Ferroelectric Polymers* (Chapman Hall, New York, 1988).
[4] The best modern synthesis techniques produce films with crystallinity of about 60%. See K. Nakamura, D. Sawai, Y. Watanabe, D. Taguchi, Y. Takahashi, T. Furukawa, and T. Kanamoto, J. Polym. Sci., Part B: Polym Phys. **41**, 1701 (2003).
[5] M. Poulsen and S. Ducharme, IEEE Trans. Dielec. Elec. Insul. (to be published).
[6] R. G. Kepler and R. A. Anderson, J. Appl. Phys. **49**, 1232 (1978).
[7] K. Tashiro, K. Takano, M. Kobayashi, Y. Chatani, and H. Tadokoro, Polymer **22**, 1312 (1981).
[8] A. J. Lovinger, G. T. Davis, T. Furukawa, and M. G. Broadhurst, Macromolecules **15**, 323 (1982).
[9] T. Yagi, M. Tatemoto, and J. Sako, Polym. J. (Tokyo, Jpn.) **12**, 209 (1980).
[10] K. Koga and H. Ohigashi, J. Appl. Phys. **59**, 2142 (1986).
[11] E. Bellet-Amalric and J. F. Legrand, Eur. Phys. J. B **3**, 225 (1998).
[12] K. Noda, K. Ishida, A. Kubono, T. Horiuchi, H. Yamada, and K. Matsushige, Jpn. J. Appl. Phys., Part 1 **40**, 4361 (2001).
[13] K. Noda, K. Ishida, A. Kubono, T. Horiuchi, H. Yamada, and K. Matsushige, J. Appl. Phys. **93**, 2866 (2003).
[14] K. Noda, K. Ishida, T. Horiuchi, K. Matsushige, and A. Kubono, J. Appl. Phys. **86**, 3688 (1999).
[15] T. Furukawa, Phase Transitions **18**, 143 (1989).
[16] K. Tashiro, in *Ferroelectric Polymers*, edited by H. S. Nalwa (Dekker, New York, 1995), p. 63.
[17] S. Ducharme, S. P. Palto, and V. M. Fridkin, in *Ferroelectric and Dielectric Thin Films*, edited by H. S. Nalwa (Academic Press, San Diego, 2002), Vol. 3, p. 545.
[18] K. M. Rabe, C. H. Ahn, and J.-M. Triscone, *Physics of Ferroelectrics: A Modern Perspective* (Springer-Verlag, Berlin, 2007).
[19] T. Furukawa, Ferroelectrics **57**, 63 (1984).
[20] G. Vizdrik, S. Ducharme, V. M. Fridkin, and S. G. Yudin, Phys. Rev. B **68**, 094113 (2003).
[21] B. L. Farmer, A. J. Hopfinger, and J. B. Lando, J. Appl. Phys. **43**, 4293 (1972).
[22] N. C. Banik, F. P. Boyle, T. J. Sluckin, P. L. Taylor, S. K. Tripathy, and A. J. Hopfinger, J. Chem. Phys. **72**, 3191 (1980).
[23] C. K. Purvis and P. L. Taylor, J. Appl. Phys. **54**, 1021 (1983).

[24] R. Al-Jishi and P. L. Taylor, J. Appl. Phys. **57**, 902 (1985).
[25] S. Ikeda and H. Suda, Phys. Rev. E **56**, 3231 (1997).
[26] J. Bernholc, S. M. Nakhmanson, M. B. Nardelli, and V. Meunier, Comput. Sci. Eng. **6**, 12 (2004).
[27] S. M. Nakhmanson, M. Buongiorno Nardelli, and J. Bernholc, Phys. Rev. Lett. **92**, 115504 (2004).
[28] S. M. Nakhmanson, M. Buongiorno Nardelli, and J. Bernholc, Phys. Rev. B **72**, 115210 (2005).
[29] M. Poulsen, Ph.D. thesis, University of Nebraska, 2007.
[30] N. J. Ramer and K. A. Stiso, Polymer **46**, 10431 (2005).
[31] N. J. Ramer, C. M. Raynor, and K. A. Stiso, Polymer **47**, 424 (2006).
[32] N. J. Ramer, T. Marrone, and K. A. Stiso, Polymer **47**, 7160 (2006).
[33] C. N. Borca, S. Adenwalla, J. Choi, P. T. Sprunger, S. Ducharme, L. Robertson, S. P. Palto, J. Liu, M. Poulsen, V. M. Fridkin, H. You, and P. A. Dowben, Phys. Rev. Lett. **83**, 4562 (1999).
[34] R. Blinc and B. Zeks, *Soft Modes in Ferroelectrics and Antiferroelectrics* (North-Holland, Amsterdam, 1974).
[35] D. J. Singh, Phys. Rev. B **52**, 12559 (1995).
[36] C. Lasota, C.-Z. Wang, R. Yu, and H. Krakauer, Ferroelectrics **194**, 109 (1997).
[37] P. Ghosez, E. Cockayne, U. V. Waghmare, and K. M. Rabe, Phys. Rev. B **60**, 836 (1999).
[38] M. Fornari and D. J. Singh, Phys. Rev. B **63**, 092101 (2001).
[39] R. Hasegawa, Y. Takahashi, Y. Chatani, and H. Tadokoro, Polym. J. (Tokyo, Jpn.) **3**, 600 (1972).
[40] J. C. Li, R. Q. Zhang, C. L. Wang, and N. B. Wong, Phys. Rev. B **75**, 155408 (2007).
[41] C.-G. Duan, W. N. Mei, J. R. Hardy, S. Ducharme, J. Choi, and P. A. Dowben, Europhys. Lett. **61**, 81 (2003).
[42] Many authors employ nonstandard *Cm*2*m* and *Cc*2*m* symmetry settings for the planar zigzag and alternately deflected β-PVDF structural models, respectively. Yet, even more frequently authors do not specify exactly what symmetry they use. See, e.g., Ref. 30 for a more extended discussion of symmetries.
[43] M. Bai, X. Z. Li, and S. Ducharme, J. Phys.: Condens. Matter **19**, 196211 (2007).
[44] QUANTUM ESPRESSO is available from http://www.quantum-espresso.org; see also, P. Giannozzi, S. Baroni, N. Bonini, M. Calandra, R. Car, C. Cavazzoni, D. Ceresoli, G. L. Chiarotti, M. Cococcioni, I. Dabo, A. D. Corso, S. de Gironcoli, S. Fabris, G. Fratesi, R. Gebauer, U. Gerstmann, C. Gougoussis, A. Kokalj, M. Lazzeri, L. Martin-Samos, N. Marzari, F. Mauri, R. Mazzarello, S. Paolini, A. Pasquarello, L. Paulatto, C. Sbraccia, S. Scandolo, G. Sclauzero, A. P. Seitsonen, A. Smogunov, P. Umari, and R. M. Wentzcovitch, J. Phys.: Condens. Matter **21**, 395502 (2009).
[45] D. Vanderbilt, Phys. Rev. B **41**, 7892 (1990).
[46] S. Baroni, S. de Gironcoli, A. D. Corso, and P. Giannozzi, Rev. Mod. Phys. **73**, 515 (2001).
[47] J. P. Perdew, K. Burke, and M. Ernzerhof, Phys. Rev. Lett. **77**, 3865 (1996).
[48] H. J. Monkhorst and J. D. Pack, Phys. Rev. B **13**, 5188 (1976).
[49] PQS version 3.3, Parallel Quantum Solutions, 2013 Green Acres Road, Fayetteville, Arkansas 72703.
[50] 6 Gaussian functions describing the inner-shell orbital, double zeta with 3 and 1 Gaussian functions, respectively, for the valence orbital; additional polarization and diffuse functions on all atoms.
[51] W. J. Hehre, R. Ditchfield, and J. A. Pople, J. Chem. Phys. **56**, 2257 (1972).
[52] P. C. Hariharan and J. A. Pople, Theor. Chim. Acta **28**, 213 (1973).
[53] Z.-Y. Wang, K.-H. Su, H.-Q. Fan, and Z.-Y. Wen, Polymer **48**, 7145 (2007).
[54] A. P. Scott and L. Radom, J. Phys. Chem. **100**, 16502 (1996).
[55] M. W. Wong, Chem. Phys. Lett. **256**, 391 (1996).
[56] J. B. Foresman and A. Frisch, *Exploring Chemistry with Electronic Structure Methods* (Gaussian, Pittsburgh, 1996).
[57] J. P. Merrick, D. Moran, and L. Radom, J. Phys. Chem. A **111**, 11683 (2007).
[58] More sophisticated methods are available for obtaining better agreement between theoretical and experimental frequencies. For example, the scaled-quantum-mechanical (SQM) procedure rescales the force field rather than the frequencies and utilizes different scaling factors for various kinds of vibrations (stretching, bending, torsion, etc.), see P. Pulay, G. Fogarasi, G. Pongor, J. E. Boggs, and A. Vargha, J. Am. Chem. Soc. **105**, 7037 (1983); and J. Baker, A. A. Jarzecki, and P. Pulay, J. Phys. Chem. A **102**, 1412 (1998). In this investigation we have chosen simplicity over accuracy but nevertheless found the SQM software helpful for performing the PED analysis.
[59] K. Tashiro, Y. Itoh, M. Kobayashi, and H. Tadokoro, Macromolecules **18**, 2600 (1985).
[60] M. Kobayashi, K. Tashiro, and H. Tadokoro, Macromolecules **8**, 158 (1975).
[61] R. Korlacki, J. T. Johnson, J. Kim, S. Ducharme, D. W. Thompson, V. M. Fridkin, Z. Ge, and J. M. Takacs, J. Chem. Phys. **129**, 064704 (2008).
[62] To put our work into a proper historical perspective, we should note that the first calculation of phonon-band dispersions in PVDF was done in 1979 by utilizing an empirical force-field model for molecular chains. See Ch. Seidel, Acta Polym. **30**, 490 (1979).
[63] Herman, T. Uno, A. Kubono, S. Umemoto, T. Kikutani, and N. Okui, Polymer **38**, 1677 (1997).
[64] Herman, S. Umemoto, T. Kikutani, and N. Okui, Polym. J. (Tokyo, Jpn.) **30**, 659 (1998).
[65] M. Hanesaka and K. Tashiro, Macromolecules **35**, 10210 (2002).
[66] B. Ameduri, C. Ladavière, F. Delolme, and B. Boutevin, Macromolecules **37**, 7602 (2004).
[67] F. Montefusco, R. Bongiovanni, A. Priola, and B. Ameduri, Macromolecules **37**, 9804 (2004).
[68] C. Boyer, D. Valade, L. Sauguet, B. Ameduri, and B. Boutevin, Macromolecules **38**, 10353 (2005).